Wandering Spurs in MASH 1-1 Delta-Sigma Modulators

Yann Donnelly, *Student Member, IEEE,* and Michael Peter Kennedy, *Fellow, IEEE*

***Abstract*—Wandering spurs are a little-studied phenomenon seen in MASH and SQ-DDSM modulators. They take the form of frequency-modulated spurs which periodically appear in-band. Since modulators are often employed as divide ratio controllers in fractional-*N* phase lock loops, these spurs can feed into the output phase noise spectrum. In this paper we explain the mechanism which creates the wandering spurs, and offer a prediction for the behavior of these spurs in the MASH 1-1 modulator. Simulation results are presented which confirm our theoretical predictions.**

***Index Terms*—wandering spur, PLL, MASH, experimental, modulator, delta-sigma, phase noise, spectrum, spur, phase lock loop, frequency modulation.**

I. Introduction

SPURIOUS frequency components ("spurs") are a much-studied phenomenon in the literature on fractional-*N* PLLs. Two common spurs are the reference spur at f_{PFD} and fractional spurs at multiples of $(x/M) \times f_{\text{PFD}}$, where x and M are the modulator input and modulus, respectively. These spurs respectively arise from direct reference clock feed-through and from the excitation of loop nonidealities by phase noise introduced by the divide ratio modulator [1]–[3]. The former is usually attenuated by the loop response, while the latter may be located in the passband of the loop response, in which case it is a significant component of the PLL output phase noise [4]. Fig. 1 shows PLL output phase noise spectra demonstrating both types of spurs.

A new phenomenon, termed the Wandering Spur, has been described in the frequency synthesizer literature recently [5], although similar behavior has been previously observed in audio sigma delta modulators [6]. Unlike the aforementioned reference and fractional spurs, which are fixed in frequency, this is a frequency-modulated spur, and has only received scarce treatment in the literature. The prediction offered by [5] applies to the MASH 1-1-1 case and small values of x, where the behavior of the spur is complicated by the presence of an additional Digital Delta-Sigma Modulators (DDSM) stage, and does not consider the presence of wandering spur harmonics, nor does it offer a prediction for the amplitudes of these wandering spurs or consider the impact of modulator dithering. This paper aims to provide an in-depth analysis of the mechanism behind and behavior of the wandering spur in the simplest case, that of a fractional-*N* PLL employing a MASH 1-1 modulator, as well as offering a qualitative description of the wandering spur.

Y. Donnelly is with the School of Electrical and Electronic Engineering, University College Dublin, Dublin 4, Ireland, and also with the Microelectronic Circuits Centre Ireland (MCCI), based at Tyndall National Institute, Cork, Ireland. (e-mail: y.donnelly@umail.ucc.ie)

M. P. Kennedy is with the School of Electrical and Electronic Engineering, University College Dublin, Dublin 4, Ireland, and also with MCCI, Dublin, Ireland. (e-mail: peter.kennedy@ucd.ie)

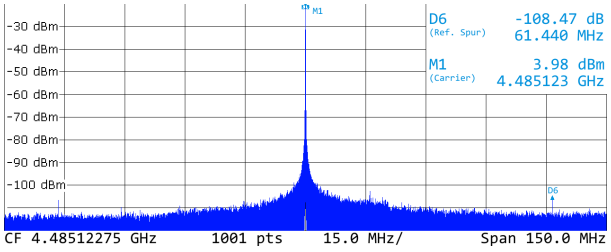

(a) Reference spurs

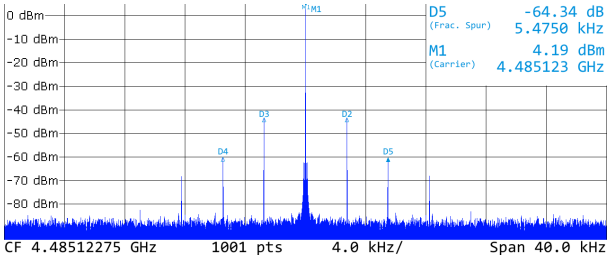

(b) Fractional spurs

Fig. 1: Spectra of (a) reference spurs, here present at $\pm 61.44\,\text{MHz}$, and (b) fractional spurs, here present at $\pm k \times 2.75\,\text{kHz}$. Here, $f_{\text{PFD}} = 61.44\,\text{MHz}$, $x = 1500$ and $M = 2^{25}$.

The paper is organized as follows. Section II provides an overview of the theory behind the MASH 1-1 modulator, while Section III demonstrates the wandering spur and presents its key characteristics. Section IV then builds on the description of the MASH to demonstrate the generation of wandering spurs in an example scenario, before developing this into a general expression for wandering spurs. Section V verifies the theoretical exposition through simulation, and conclusions are presented in Section VI.

II. The MASH modulator

The wandering spur can be demonstrated easily in simulation. The simplest setup which produces a wandering spur is an undithered MASH 1-1 modulator. For this reason, we will begin by describing this structure.

The MASH modulator is the most widely used modulator in fractional-N PLLs [7]. Consisting of a cascade of daisy-chained DDSM, it offers an area-efficient solution with a high degree of noise shaping. In this section we will begin by summarizing the theory of operation of the DDSM, before building on this to describe the MASH modulator.

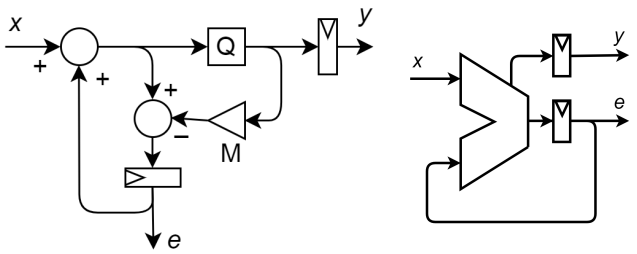

(a) (b)

Fig. 2: (a) Diagram of first-order DDSM; (b) First-order DDSM implemented using an adder with carry out.

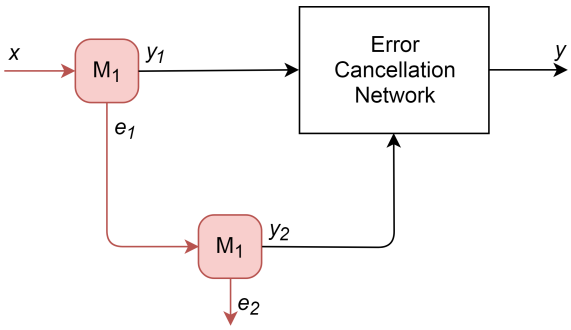

Fig. 3: Schematic of a MASH 1-1.

A. DDSM theory of operation

The DDSM is a noise-shaping modulator which consists of a multibit quantizer in a feedback loop. A DDSM with a 1-bit output is shown in Fig. 2(a). An error signal, e, is fed back to the input, resulting in $+20\,\mathrm{dB}$/decade noise shaping from accumulation of the error. Due to the m-bit quantization, the output mean is attenuated by a factor of $M = 2^m$ compared to the input.[1] Thus:

$$Y(z) = \frac{1}{M}\left(z^{-1}X(z) - \left(1 - z^{-1}\right)E(z)\right) \tag{1}$$

where Y, X and E denote the z-transforms of the output, input and quantization error, respectively.

The first-order DDSM block can easily be implemented using an m-bit adder as a quantizer, where the sum and carry out are equivalent to the modulator error and output, respectively, as shown in Fig. 2(b).

B. MASH theory of operation

The MASH modulator is a development of the DDSM which employs a number of quantization stages to increase the noise shaping of the error term. Fig. 3 shows a MASH 1-1, which consists of two first-order DDSMs, and an error cancellation network. Together, these implement the following transfer function:

$$Y(z) = z^{-1}Y_1(z) + \left(1 - z^{-1}\right)Y_2(z), \tag{2}$$

[1]In some modulator designs, an odd value of the modulus, M, is used. In these cases the analysis given in this paper is still valid, with suitable modification of the inequalities which will be presented as Eqs. (21), (22) and (24) later.

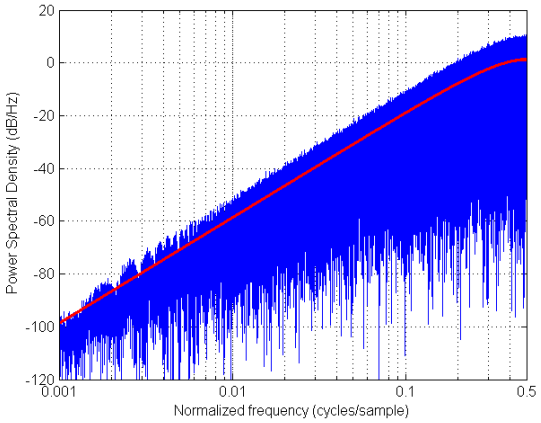

Fig. 4: Power spectral density of a 16-bit MASH 1-1, showing $+40\,\mathrm{dB}$/decade noise shaping. The theoretical prediction given by [2, Eq. (23)], which assumes a white quantization error spectrum, is shown as a solid red curve.

The error term of the first DDSM is fed to a second DDSM, whose output therefore contains the error term in addition to a new error term, E_2.

$$Y_1(z) = \frac{1}{M}\left(z^{-1}X(z) - \left(1 - z^{-1}\right)E_1(z)\right), \tag{3}$$

$$Y_2(z) = \frac{1}{M}\left(z^{-1}E_1(z) - \left(1 - z^{-1}\right)E_2(z)\right). \tag{4}$$

In the error cancellation network, the second DDSM's output is accumulated and added to the first DDSM's output, cancelling the first error term and leaving behind the term due to the input and the second error term. Thus,

$$\begin{aligned} Y(z) &= z^{-1}Y_1(z) + \left(1 - z^{-1}\right)Y_2(z) \\ &= \frac{1}{M}\left(z^{-2}X(z) - \left(1 - z^{-1}\right)^2 E_2(z)\right). \end{aligned} \tag{5}$$

The error term $\left(1 - z^{-1}\right)^2 E_2$ has $+40\,\mathrm{dB}$/decade noise shaping, as shown in Fig. 4, due to the effect of the two feedback loops, which results in less in-band noise after low-pass filtering.

The MASH can be implemented using L first-order DDSM blocks and a suitably corrected error cancellation network if a different order of noise shaping is required. In each case, the modulation phase noise is dictated by the final error term, $\left(1 - z^{-1}\right)^L E_L$.

C. Contribution of e_2 to the PLL output phase noise

This paper considers the use of a MASH 1-1 as the divide ratio controller in a fractional-*N* PLL, the architecture of which is shown in Fig. 5. The input of the MASH is chosen such that the desired divide ratio is equal to the $z^{-2}X(z)/M$ term in Eq. (5). The modulator contributes shaped phase noise due to the remaining $\left(1 - z^{-1}\right)^2 E_2(z)/M$ term [2].

The loop architecture has the effect of accumulating the noise term added to the loop, which reduces the degree of noise shaping to $+20\,\mathrm{dB}$/decade. The frequency spectrum of

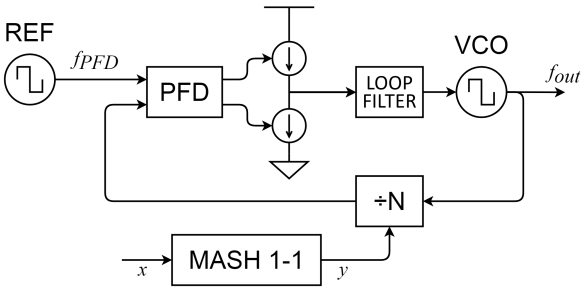

Fig. 5: Structure of a fractional-N PLL employing a MASH 1-1 as its divide ratio controller.

TABLE I: MASH 1-1 example used in Figs. 6–9.

x	1
M	2^{18}
N_{FFT}	2^{11}
Overlap	50%

the contribution of the MASH modulator to the PLL output phase noise can be expressed as [2]:

$$\phi_{\text{out, mod}}(z) = \frac{2\pi}{M f_{\text{PFD}}} \left(1 - z^{-1}\right) G(z) E_2(z), \qquad (6)$$

where $G(z)$ is the closed loop response of the PLL.

It can be seen from Eq. (6) that the spectrum of the output phase noise due to the modulator is an amplified version of the spectrum of e_2, with $+20\,\text{dB/decade}$ spectral shaping and shaping by the low-pass loop response $G(z)$. We can treat e_2 as a proxy for the output phase noise due to the modulator; this will allow us to study the wandering spurs clearly in the absence of the filter terms $\left(1 - z^{-1}\right) G(z)$.

III. Description of the Wandering Spur

The wandering spur is observed as a succession of frequency-modulated spurs that move towards and away from the carrier frequency. These spurs are symmetrical about the carrier frequency, and are most visible when they are inside the passband of the closed loop transfer function, where they are not attenuated by the loop response.

A. Conditions producing wandering spurs

The rate of change of the spur frequency is closely related to the fractional component of the divide ratio, i.e. the input to the modulator. This would suggest that the modulator is the source of the phenomenon, which has been confirmed in [5].

The modulus of the modulator should be made relatively large, e.g. $M \geq 2^{16}$, and the input, x, set to a value close to, but not equal to, 0, M or a fraction of the modulus (for example, $x = 1$ or $x = M/2 + 1$ are suitable). These values will ensure slow-moving wandering spurs which are easy to see in the spectra.

The FFT size for observing the power spectrum should be carefully chosen so as to ensure that there is sufficient temporal resolution that the movement of the spur is captured, but also sufficient frequency resolution that different wandering spurs can be distinguished. The use of a large modulus will ensure that both are easily obtainable.

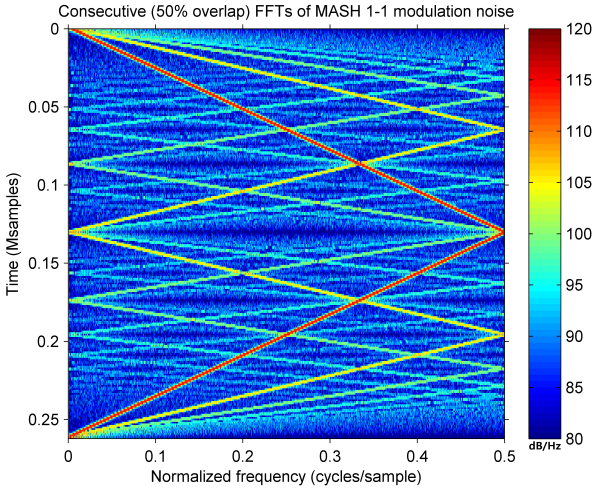

(a) Spectrogram of e_2.

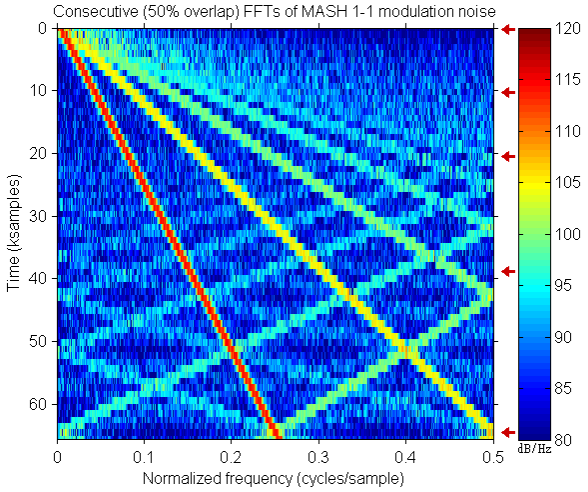

(b) Cropped spectrogram, showing multiple harmonic components.

Fig. 6: Example spectrogram of MASH 1-1 error term e_2 showing wandering spurs, from a MATLAB simulation of a MASH 1-1 modulator. The wandering spur, and its harmonics, are seen to move from DC out to higher frequencies, folding back to DC after reaching $0.5\,\text{cycles/sample}$.

B. Wandering spur examples

Fig. 6 shows a spectrogram of the second error term, e_2, of a simulated MASH 1-1 modulator using the setup described in Table I; the reason for focusing on the unfiltered spectrum, e_2, has been explained in Section II-C. Fig. 7 shows the equivalent PLL output phase noise spectrum, in which the same wandering spurs are clearly seen. However, the distortion introduced by the $(1 - z^{-1})$ and $G(z)$ terms makes such pictures harder to interpret. Therefore we will henceforth show spectra of e_2 rather than the output phase noise.

Each FFT is 2^{11} samples long and adjacent FFTs overlap by 50%. There is therefore a time delay of 2^{10} samples between successive FFTs. The spectrogram in Fig. 6(a) clearly shows wandering spurs moving between the carrier and the Nyquist frequency ($f_{\text{ref}}/2$), the most pronounced of which is dark red.

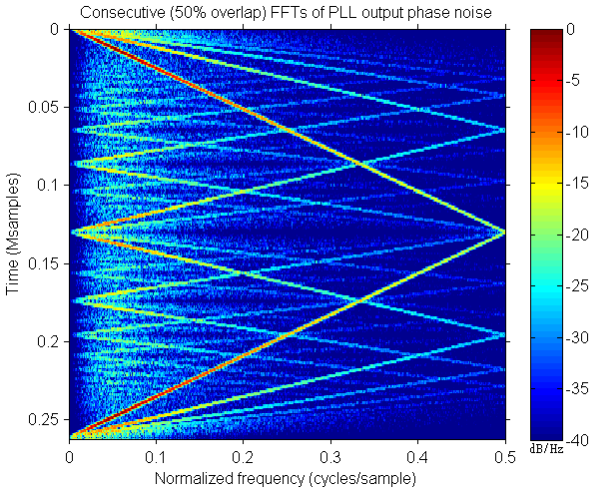

Fig. 7: Spectrogram of PLL output phase noise corresponding to the situation shown in Fig. 6(a). The positions of the wandering spurs are identical; however, their amplitudes are distorted by numerous transfer functions, and the weaker harmonics are less well defined. For this reason we will henceforth be showing spectrograms of e_2.

A cropped version, shown in Fig. 6(b), shows a number of separate, linearly frequency-modulated spurs. The dominant spur (shown in red) is the slowest-moving, with a wander rate of approximately $0.25/65\,536\,\mathrm{cycles/sample}$ per sample period, while the remaining spurs have wander rates which are integer multiples of this.

Figs. 8(a)–(d) show spectra taken at time offsets of 0, 10 240, 20 480 and 38 912 samples, respectively, indicated by the red arrows in Fig. 6(b). These spectra show the movement of the wandering spurs from DC to the Nyquist frequency. Each FFT is calculated over 2^{11} samples, during which time each individual spur has moved a fixed distance, with the fundamental spur moving at $7.8 \times 10^{-3}\,\mathrm{cycles/sample}$. This results in each spur creating a *ridge* of width $k \times 7.8 \times 10^{-3}\,\mathrm{cycles/sample}$ in the FFT, where k is the order of the harmonic, and not a peak as would be expected from a spur of fixed frequency.

In Fig. 8(d), which is taken at a time offset of 38 912 samples, some folding has taken place. The fundamental is present at $0.15\,\mathrm{cycles/sample}$, which would place the 4th and 5th harmonics at $0.60\,\mathrm{cycles/sample}$ and $0.75\,\mathrm{cycles/sample}$, respectively. They instead show up at $0.4\,\mathrm{cycles/sample}$ and $0.25\,\mathrm{cycles/sample}$, respectively, and have started wandering back to DC, due to folding.

Fig. 8(e) shows a spectrum taken at a time offset of 65 536 samples. This spectrum shows the situation where the 2nd harmonic reaches the Nyquist frequency, and the 4th harmonic hovers around DC, as can be seen by the increased noise power at low frequencies. The fundamental and 3rd and 5th harmonics are superimposed at $0.25\,\mathrm{cycles/sample}$; since each has a different wander rate and amplitude, this results in the formation of a 3-tier pyramidal shape at this frequency. This is shown clearer in the cropped spectrum of Fig. 9.

These spectra all show the case where there is one fun-

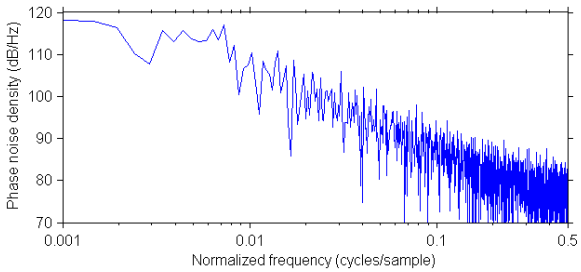

(a) $n = 0$

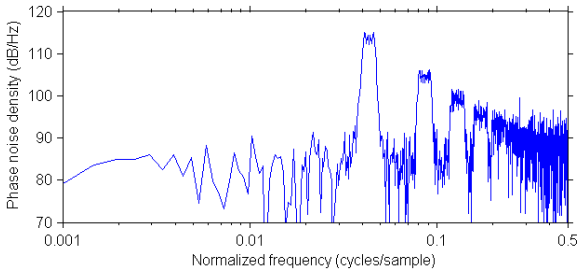

(b) $n = 10\,240$

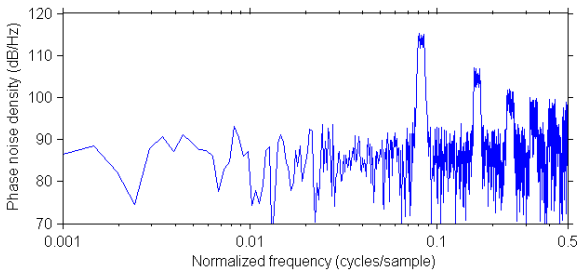

(c) $n = 20\,480$

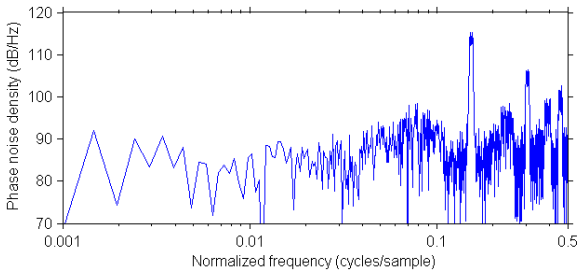

(d) $n = 38\,912$

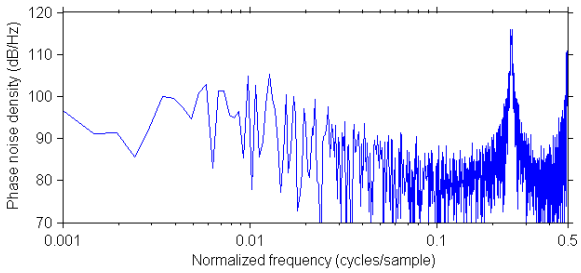

(e) $n = 65\,536$

Fig. 8: Spectra of e_2 taken at five different moments in time, each corresponding to the points indicated by each of the arrows on Fig. 6(b).

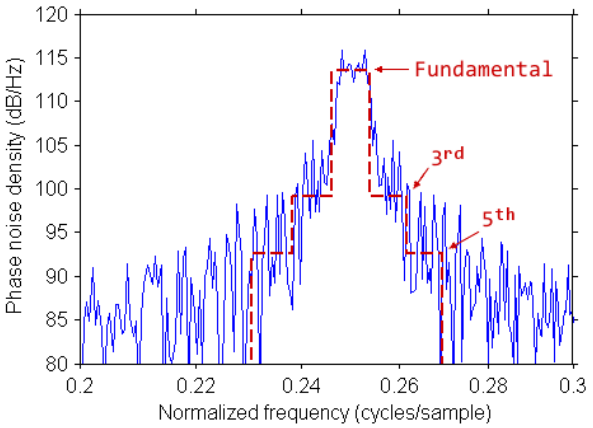

Fig. 9: Main peak of Fig. 8(e), showing overlapping wandering spurs with different amplitudes and wander rates. The prediction, shown dashed, is explained in Appendix A.

damental moving spur with accompanying harmonics. At certain modulator inputs far from 0 or M, multiple groups of wandering spurs are also possible. Fig. 10 shows a spectrogram for the input $x = (M/4) - 1$, showing 4 groups of wandering spurs, each containing a single fundamental component and harmonics with lower amplitudes and faster wander rates.

C. The wandering spur is not a simulation artifact

It is important to note that the simulated modulator is a basic MASH 1-1, consisting only of accumulators, subtractors and delays in a feed-forward architecture. Furthermore, the modulator is undithered; therefore this phenomenon is not an artifact of a random noise generator. It is also not an artifact of the spectral analysis method, as the wandering spur behaves identically, regardless of the FFT parameters, once the spectrum has sufficient time and frequency resolution to show it clearly.

Fig. 11 shows three spectrograms of the error term shown in Fig. 6(a), using different FFT lengths. Doubling the FFT length has the effect of doubling the frequency resolution while also halving the temporal resolution; it also increases the heights of the spur peaks by $\sim 9\,\mathrm{dB}$. As can be seen in these spectrograms, the behavior of the wandering spur is otherwise unaffected by the change in FFT parameters.

D. Empirical observations

Several empirical observations can be made about wandering spurs caused by a MASH 1-1:

- They occur when the fractional component of the input to the modulator, x, approaches a fraction of the modulus, aM/b, where the denominator b is small. The wander rate is proportional to the distance between x and aM/b.
- There may be one fundamental wandering spur, when x is close to 0 or M, or there may be multiple wandering spur groups, each with their own fundamental spur. In the latter case, the fundamental spurs all have equal amplitudes and wander rates, and are equally spaced in time.

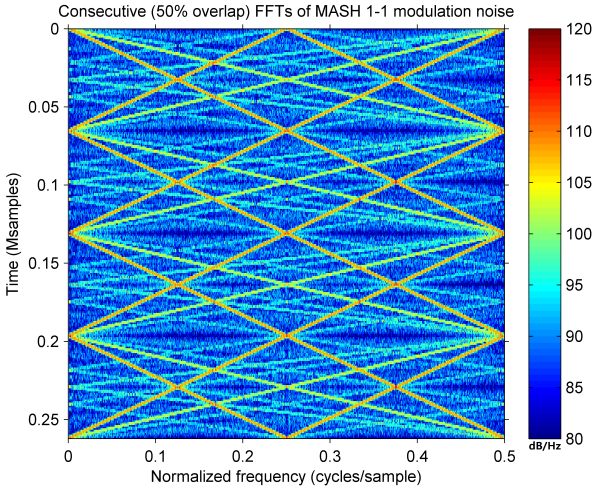

(a) Long-term spectrum.

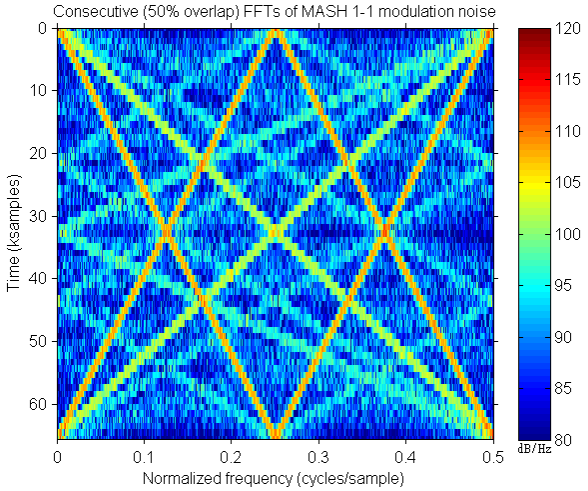

(b) Short-term spectrum, showing multiple harmonic components.

Fig. 10: Spectrogram of MASH 1-1 error term e_2 with $x = (M/4) - 1$, showing four independent wandering spur groups.

- The amplitudes of the harmonics decrease regularly and monotonically with the wander rate. Furthermore, no harmonics are missing, which would suggest that the system is modulated by a sawtooth waveform.

IV. Analysis of Wandering Spurs in the MASH 1-1

The MASH 1-1 inherently produces wandering spurs. In order to understand why, we return to the description of the MASH modulator and study the effect of the input on e_2. The structure of the MASH 1-1 is repeated in Fig. 12(a), with typical waveforms shown as Fig. 12(b).

A. Frequency modulation in the DDSM

We demonstrated in Section II-A that the DDSM can be described as an m-bit adder, where the error term e is equivalent to the m-bit output without carry. We can therefore represent e in terms of the input, x, as follows:

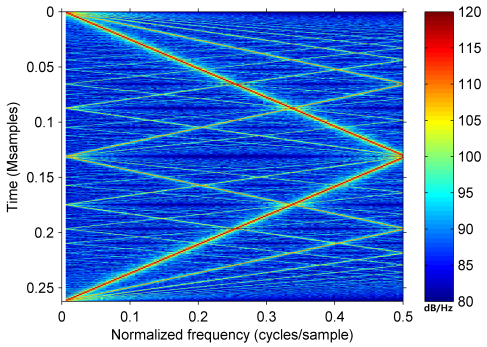

(a) $N_{\text{FFT}} = 2^8$

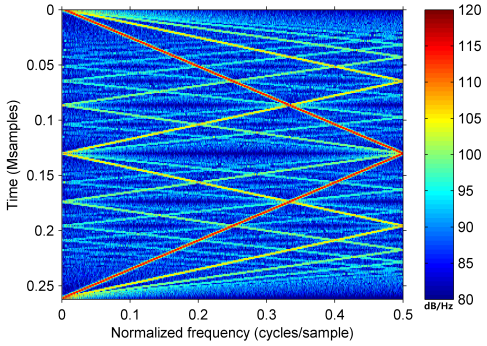

(b) $N_{\text{FFT}} = 2^{11}$

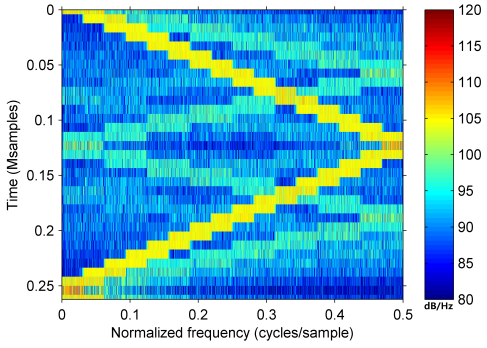

(c) $N_{\text{FFT}} = 2^{14}$

Fig. 11: Spectrogram of MASH 1-1 error term e_2 under different FFT conditions. The wander rates are not influenced by the FFT parameters; the heights of the spur peaks decrease as N_{FFT} decreases, due to peak spreading, but the actual spur powers remain constant.

$$e[n] = \left(e[0] + \sum_{k=1}^{n-1} x[k] \right) \pmod{M}. \tag{7}$$

If the input is held constant, then e will take the form of a sawtooth waveform. This is due to a digital overflow which occurs when $e[n-1] + x[n-1] > M$. The fundamental frequency of this waveform is:

$$f_e = \frac{x}{M}. \tag{8}$$

In the more general case, with a time-varying input x, we can likewise define the *instantaneous* frequency of e:

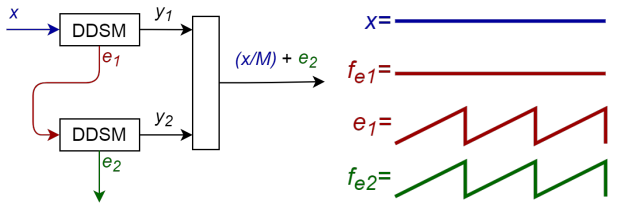

(a) (b)

Fig. 12: Structure of the MASH 1-1 (a), and important waveforms when there is a constant input x (b).

$$f_e[n] = \frac{x[n-1]}{M}. \tag{9}$$

We can explain the operation of the DDSM, with respect to the x and e terms, as follows:

Observation IV.1. The DDSM produces a sawtooth waveform, e, which is frequency-modulated by the input, x.

B. Frequency modulation in the MASH 1-1

In the constant-input MASH, this mechanism produces an error signal in the first DDSM, e_1, with a fixed frequency $f_{e_1} = x/M$. This signal then frequency-modulates the error term of the second DDSM, e_2, resulting in a waveform with instantaneous frequency $f_{e_2}[n] = e_1[n]/M$, as shown in Fig. 12. Therefore, the error term of the second DDSM contains moving frequency components, i.e. wandering spurs.

In the MASH 1-1, the output is given by:

$$Y(z) = \frac{1}{M}\left(z^{-2}X(z) - \left(1 - z^{-1}\right)^2 E_2(z) \right). \tag{10}$$

In other words, the error term in the output is proportional to the shaped error signal of the second DDSM, e_2. Therefore, the aforementioned wandering spurs will be present in the output of the MASH 1-1 modulator, and by extension, in the output phase noise spectrum of the PLL.

We can see the influence of e_1 on the frequency of e_2 by direct examination of their waveforms. In Fig. 13(a), e_1 slowly increases in value from 0 to 2000, producing a corresponding decrease in the period of e_2. Around $n = 1000$, e_2 has a period of roughly $1000/2^{18} \simeq 262$ samples.

As e_1 approaches $M/2$, shown in Fig. 13(b), e_2 begins to overflow roughly every second sample period; thus, over *two* sample periods e_2 increases roughly $2(M/2) \equiv 0 \pmod{M}$. This results in a situation at $n = M/2$ where e_2 moves in an oscillatory fashion between roughly $M/4$ and $3M/4$, as seen in Fig. 13(c).

As e_1 increases past $M/2$, the rate of increase of e_2 over two sample periods exceeds M, and hence:

$$2(e_1) \equiv k \pmod{M}, \quad -\frac{M}{2} \leq k \leq 0 \tag{11}$$

Thus, the rate of increase of e_2 appears to *decrease*, rather than increase, with increasing e_1, until the situation is reached in Fig. 13(d) where $n = M \equiv 0 \pmod{M}$, and the rate of change of e_2 reaches 0. At this point e_1 overflows and the cycle is repeated.

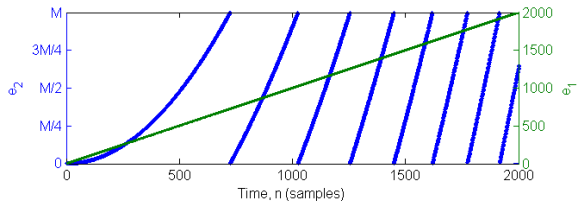

(a) $n = 0$

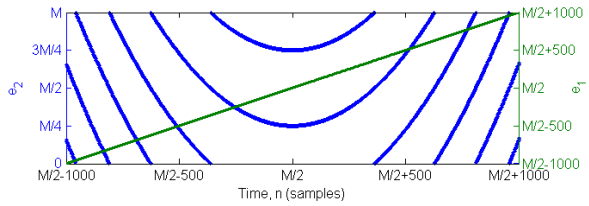

(b) $n = M/2$

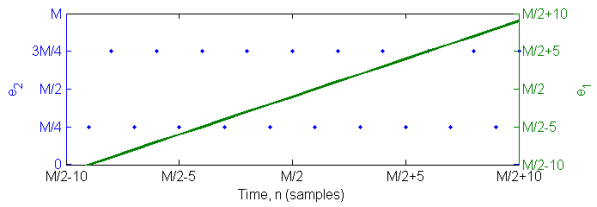

(c) $n = M/2$

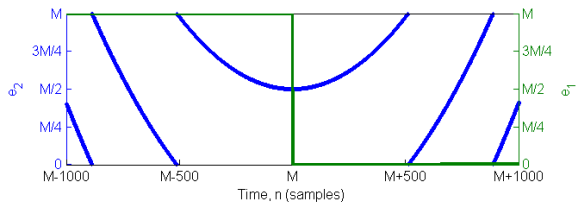

(d) $n = M$

Fig. 13: MASH 1-1 error term waveforms at times (a) $n = 0, \ldots, 2000$, showing the frequency of e_2 linearly increasing with time, (b) n near $M/2$, where the frequency reaches a maximum of $0.5\,\text{cycles/sample}$, (c) ditto, cropped, and (d) n near M, where the frequency reduces to 0 before increasing once more. $x = 1$ and $M = 2^{18}$ in all plots.

C. Wandering spur example

Before presenting a general expression for the wandering spur in the MASH 1-1 modulator, we apply the insight obtained in the previous section to a simple example. The goal is to show clearly how the deterministic operation of a daisy chain of DDSM blocks (and consequently *every* MASH divider controller) inherently produces wandering spurs.

Consider the case where the input is close to a fraction of the modulus:

$$x = \frac{M}{4} + 1. \tag{12}$$

The error term of the first DDSM therefore takes on the following form (applying the initial condition $e_1[-1] = 0$):

$$e_1[n-1] = \Big(0 + 0,\ \frac{M}{4} + 1,\ \frac{M}{2} + 2,\ \frac{3M}{4} + 3, \tag{13}$$

$$0 + 4,\ \frac{M}{4} + 5,\ \frac{M}{2} + 6,\ \frac{3M}{4} + 7,\ \ldots\Big). \tag{14}$$

Since e_1 is the input to the second DDSM, and using (9) above, we obtain:

$$f_{e_2}[n] = \Big(0 + 0,\ \frac{1}{4} + \frac{1}{M},\ \frac{1}{2} + \frac{2}{M},\ \frac{3}{4} + \frac{3}{M}, \tag{15}$$

$$0 + \frac{4}{M},\ \frac{1}{4} + \frac{5}{M},\ \frac{1}{2} + \frac{6}{M},\ \frac{3}{4} + \frac{7}{M},\ \cdots\Big), \tag{16}$$

where terms that are close to each other are colored similarly.

It should be noted that the terms due to the '$M/4$' component cycle quickly between $0, 1/4, 1/2$ and $3/4$, while the terms due to the '1' component increase slowly and linearly. Since the '$k/4$' components cycle very quickly, the waveform of e_1 appears to consist of 4 separate signals, equally spaced by $1/4\,\text{cycles/sample}$. The resulting spectrum of e_2 will thus appear to contain 4 separate wandering spur groups, corresponding to the $0, 1/4, 1/2$ and $3/4$ terms, respectively. Thus, we can approximate each of these wandering spur groups through interpolation:

$$f^0_{e_2}[n] = \Big(0, \frac{1}{M}, \frac{2}{M}, \frac{3}{M}, \frac{4}{M}, \frac{5}{M}, \frac{6}{M}, \frac{7}{M}, \ldots\Big), \tag{17}$$

$$f^1_{e_2}[n] = \frac{1}{4} + \Big(0, \frac{1}{M}, \frac{2}{M}, \frac{3}{M}, \frac{4}{M}, \frac{5}{M}, \frac{6}{M}, \frac{7}{M}, \ldots\Big), \tag{18}$$

$$f^2_{e_2}[n] = \frac{1}{2} + \Big(0, \frac{1}{M}, \frac{2}{M}, \frac{3}{M}, \frac{4}{M}, \frac{5}{M}, \frac{6}{M}, \frac{7}{M}, \ldots\Big), \tag{19}$$

$$f^3_{e_2}[n] = \frac{3}{4} + \Big(0, \frac{1}{M}, \frac{2}{M}, \frac{3}{M}, \frac{4}{M}, \frac{5}{M}, \frac{6}{M}, \frac{7}{M}, \ldots\Big). \tag{20}$$

It can be seen that each term increases linearly. However, due to the discrete-time operation of the DDSM, the spectrum is folded down into the $[0, 0.5]$ region. Therefore, each group of spurs will appear to move linearly back and forth between DC ($f = 0$) and the Nyquist frequency ($f = 0.5$).

Consequently, we can represent the motion of the wandering spurs using the following function, which is periodic with period M:

$$f^k_{e_2}[n] = \begin{cases} \dfrac{n}{M} - \dfrac{k}{4}, & 0 \le \big(n - n^k_0\big) < \dfrac{M}{2}, \\ 1 - \dfrac{n}{M} + \dfrac{k}{4}, & \dfrac{M}{2} \le \big(n - n^k_0\big) < M, \end{cases} \tag{21}$$

where $0 \le k < 4$ and $n^k_0 = (kM)/4$.

The fundamental frequency of the first spur will hence take the form:

$$f^0_{e_2}[n] = \begin{cases} \dfrac{n}{M}, & 0 \le n < \dfrac{M}{2}, \\ 1 - \dfrac{n}{M}, & \dfrac{M}{2} \le n < M. \end{cases} \tag{22}$$

It is worth re-iterating that this phenomenon produces a *single* time-varying frequency component, which has *the appearance of* multiple wandering spurs due to the harmonic relationship between x and M.

D. The general case

The same approach can be used to determine a general expression for the wandering spur in the MASH 1-1 modulator.

We start by assuming that the input is held constant, and describing it as the sum of two terms, $x = x' + \bar{d}$, where the first term is related to the modulus as follows:

$$x' = \frac{aM}{b} \qquad a, b \in \mathbb{Z}, (a, b) \text{ coprime.} \tag{23}$$

In the above expression, it is assumed that a/b is irreducible, which occurs when a and b are coprime. It should be noted that, in the presence of first stage input dither, the mean of the dither should be factored into x. Hence, it is possible for the value of $\bar{d}$ to be fractional.

In the case of (23), there will be b apparent wandering spur groups, the fundamental frequency of each being described by the following formula:

$$f_{e_2}^k[n] = \begin{cases} \dfrac{n\left|\bar{d}\right|}{M} - \dfrac{k}{b}, & 0 \le \left(n - n_0^k\right) < \dfrac{M}{2\left|\bar{d}\right|}, \\ 1 - \dfrac{n\left|\bar{d}\right|}{M} + \dfrac{k}{b}, & \dfrac{M}{2\left|\bar{d}\right|} \le \left(n - n_0^k\right) < \dfrac{M}{\left|\bar{d}\right|}. \end{cases} \tag{24}$$

where $0 \le k < b$ and $n_0^k = (kM)/(b|\bar{d}|)$, and the formula is periodic with period $M/\left|\bar{d}\right|$.

Since each of these waveforms is a sawtooth, there will additionally be harmonics with amplitude A_0/k and frequency kf_0, where A_0 and f_0 are the amplitude and frequency of the fundamental wandering spur of each group.

E. A qualitative description

Eq. (24) can be summarised by three observations:

Observation IV.2. When the input of a MASH 1-1, x, is close to an irreducible fraction of the modulus, aM/b, there will appear to be b wandering spurs in the modulation noise spectrum.

Observation IV.3. The period of each wandering spur increases as x approaches aM/b, and is proportional to M.

Observation IV.4. The wandering spurs will have a higher amplitude and be more widely spaced, and therefore more readily apparent, when b is smaller.

F. Using Eq. (24) to predict wandering spurs

We will use a simple example to illustrate how to predict wandering spurs. The example consists of a 20-bit MASH 1-1 modulator, in a PLL with a PFD clock frequency of $f_{\text{PFD}} = 100\,\text{MHz}$ and a desired output frequency of $f_{\text{out}} = 2.450\,000\,095\,\text{GHz}$.

These two frequencies imply a divide ratio of 24.50000095. The required input to the modulator is, therefore,

$$\begin{aligned} x &= 0.50000095 \times 2^{20} \\ &= 524288.996 \\ &\simeq 524289 \\ &= \frac{M}{2} + 1, \end{aligned} \tag{25}$$

where $1/2$ is the irreducible fraction in this case.

We can therefore proceed with $M = 2^{20}$, $a = 1$, $b = 2$ and $\bar{d} = 1$. We can see immediately from $b = 2$ that there will appear to be *two* fundamental spurs (with their respective harmonics), and the very low value of $\bar{d}/M$ guarantees that the spurs will be slow-moving, and therefore very prominent in the spectrum.

Applying these values to Eq. (24), we obtain the following predictions for each of the two fundamental spurs:

$$f_{e_2}^0[n] = \begin{cases} \dfrac{n}{2^{20}}, & 0 \le n < 2^{19}, \\ 1 - \dfrac{n}{2^{20}}, & 2^{19} \le n < 2^{20}, \end{cases} \tag{26}$$

$$f_{e_2}^1[n] = \begin{cases} \dfrac{n}{2^{20}} - \dfrac{1}{2}, & 0 \le \left(n - 2^{19}\right) < 2^{19}, \\ 1 - \dfrac{n}{2^{20}} + \dfrac{1}{2}, & 2^{19} \le \left(n - 2^{19}\right) < 2^{20}, \end{cases} \tag{27}$$

where each wandering spur is periodic with period 2^{20}.

The harmonics of the wandering spur have the same properties as those of the sawtooth wave. The frequency of the q^{th} harmonic of the k^{th} fundamental wandering spur can be determined from:

$$f_{e_2,\ q^{\text{th}}\ \text{harm.}}^k[n] = \mathcal{F}\Big[f_{e_2}^k[qn]\Big], \tag{28}$$

where $\mathcal{F}[\cdot]$ denotes the folding operation, while the amplitude will be offset from the fundamental wandering spur by $-20\log_{10}(q)$ [8]. This behavior is seen in Fig. 8(d).

G. Limit cycles and idle tones

Occasional periodic artefacts are a well-known property of Delta Sigma modulators, and these phenomena have been previously classified into two families: *limit cycles*, consisting of repeating output sequences which are not noise shaped, and *idle tones*, frequency components (or "partials") that are not present in the input signal [6]. The question arises whether wandering spurs could be considered a type of limit cycle or idle tone.

It would appear from the preceding description that wandering spurs have much in common with idle tones, and indeed much more than limit cycles. Fig. 13 shows brief sections of periodic behavior which occur at a fixed time offset, which is somewhat similar to a so-called "short" limit cycle [6], with a subtle but very important distinction: with a short limit cycle, the modulator output suddenly enters a brief limit cycle state, before suddenly returning to "normal" operation [6, Fig. 5]; the output in the examples shown in Fig. 13 gradually approaches a cyclostationary state before gradually departing from it, with no clear transition between limit cycle and non-limit cycle behavior.

We suggest that the wandering spur is a type of idle chirp tone produced by the application of a non-DC input to the final stage. Both share key properties: the instantaneous frequency of the wandering spur does not depend on the frequency of the input, but is proportional to the value of the input in the DC case (accounting for folding), and the noise shaping of the modulator is unaffected. The prediction for the frequency of the DC-input idle tone, given by [6, Eq. (1)], is identical to Eq. (8).

TABLE II: MASH 1-1 example used in Fig. 14 onwards.

M	2^{20}
N_{FFT}	2^{11}
Overlap	0%

H. Higher-order modulators

It becomes apparent from the above description that the MASH 1-1 is an ideal test case for understanding wandering spurs, as the frequency modulation arises from daisy-chaining accumulators and the output of each accumulator is clearly defined (e_1 and e_2). Other modulator types would require a somewhat more involved analysis in order to describe fully the wandering spurs arising from their use, as they either contain closely interconnected accumulations or (in the case of higher-order MASH modulators) DDSM inputs which do not increase linearly in the manner of e_1 in the MASH 1-1.

The important take-away, however, is that any modulator containing daisy-chained accumulators has the potential for producing wandering spurs. This includes all MASH modulators and both single-loop and multiloop single-quantizer $\Sigma\Delta$ modulators.

V. Simulation

A. Simulation methodology

A MATLAB simulation of a 20-bit MASH 1-1 modulator, as described in Section II, was run with various inputs. The simulated spectrograms were produced without an overlap between successive FFTs. Each spectrogram shows one entire period of the fundamental wandering spur component, with the exceptions of Figs. 16 and 17 which show one quarter period of the fundamental wandering spur component.

The predictions include the fundamental wandering spurs, defined by Eq. (24), as well as the 2nd to 64th harmonics of each, as described by Eq. (28). In order to mimic the inaccuracies of the FFT operation and to antialias the image, an amplitude-normalised Hamming window was applied to each FFT prediction, which leaves the heights and positions of the spurs unaffected. The choice of window is discussed in Appendix B.

In the next subsections we discuss various cases with small and large values of b, with and without dither.

B. $b = 2$ case

A comparison between a MATLAB simulation of the 20-bit MASH 1-1 modulator described by Table II with an input of $x = (M/2)+1$ and the prediction given above is shown in Fig. 14 at three moments in time. Fig. 14(a) shows the spectrum when e_1 is small; the prediction accurately anticipates the increase in the phase noise floor at low frequencies due to the movement of the first wandering spur group. At mid frequencies, the contribution of the wandering spurs drops below the level of the noise floor, before the phase noise rises once again at higher frequencies, due to the second wandering spur group.

Fig. 14(b) shows the situation after e_1 has increased and the spurs have moved away from DC and the Nyquist frequency.

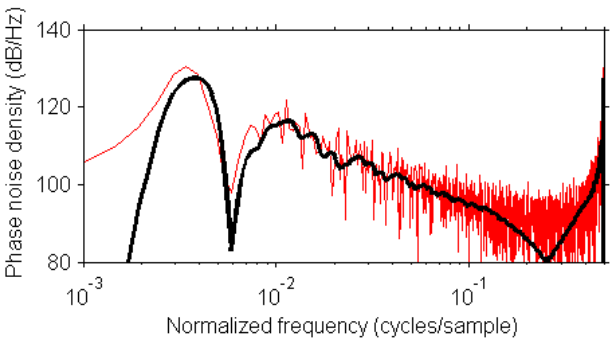

(a) $n = 2\,048$

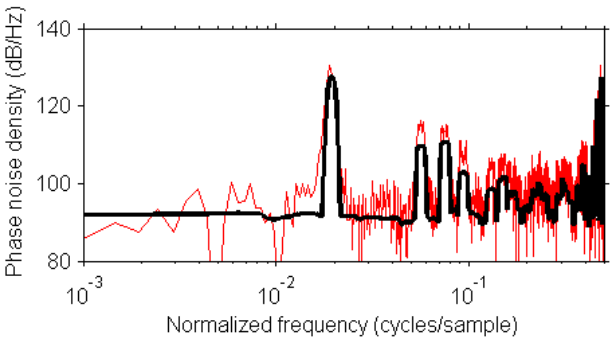

(b) $n = 18\,432$

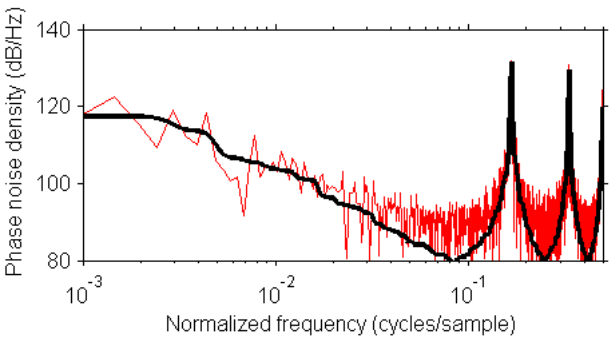

(c) $n = 174\,080$

Fig. 14: Comparison of spectra from a MATLAB simulation of a MASH 1-1 (red) and from the prediction made by (24) and (28), accounting for up to the 64th harmonic (b).

The prediction is seen to predict accurately the location, shapes and relative heights of the spurs. The prediction slightly underpredicts the phase noise contribution; this is likely because the prediction ignores the presence of a noise floor, which will increase the height of every spur whose amplitude is just above the level of the noise floor.

Fig. 14(c) shows the situation when $e_1 \simeq M/6$. This results in the superposition of all wandering spurs at DC, $f = 1/6$, $f = 1/3$ or the Nyquist frequency, similar to what was seen previously in Fig. 8(e). The prediction correctly accounts for this, in particular the way in which the combination of wandering spurs at DC with different amplitudes and wander rates results in a smooth, low-pass noise component that peaks at $117\,\text{dB/Hz}$.

The corresponding spectrograms are shown in Figs. 15 and 16. At a glance, it can be seen that the predicted positions and

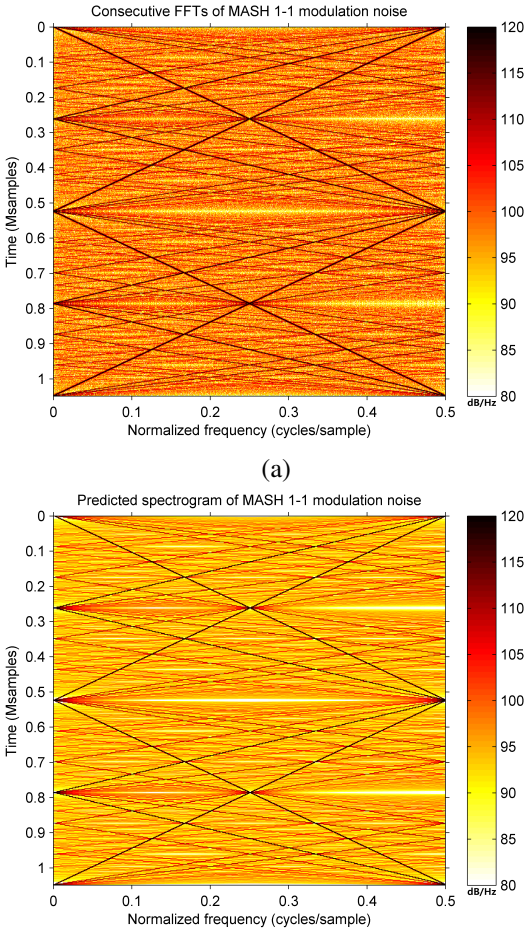

Fig. 15: Comparison between the output spectrograms from a MATLAB simulation of a MASH 1-1 (a) and from the prediction made by (24) and (28) (b).

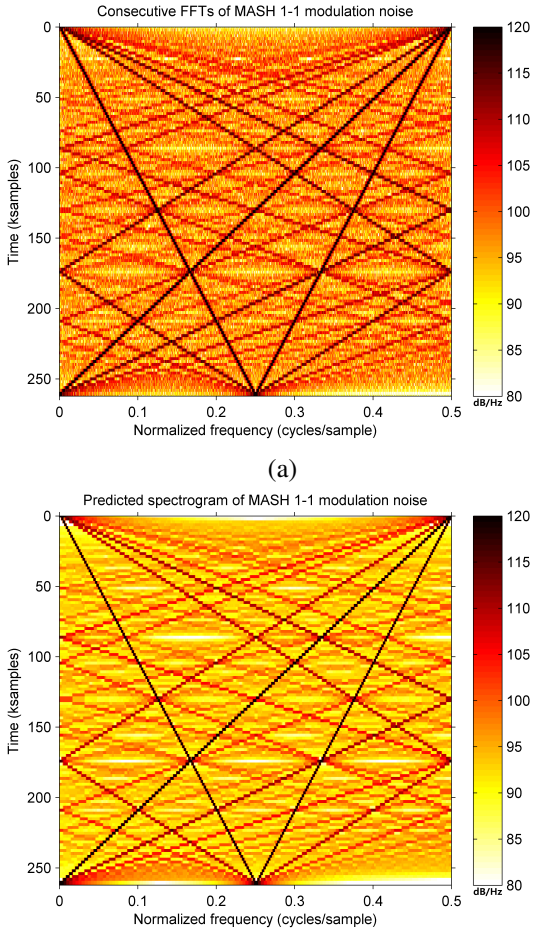

Fig. 16: Cropped view of Fig. 15, showing wandering spur components. Note the very strong doubled second harmonic component.

relative amplitudes of the wandering spurs closely resemble what is seen in simulation. Fig. 17(a) repeats the simulated waveform of Fig. 16, and shows it beside the predicted wandering spur components.

In Fig. 17(b), the first fundamental spur moves linearly from $0\,\text{cycles/sample}$ to $0.25\,\text{cycles/sample}$. All fundamental spurs are equally spaced along $0 \rightarrow 1\,\text{cycles/sample}$. Therefore, the second fundmental spur begins at $0.5\,\text{cycles/sample}$ and moves linearly to $0.75\,\text{cycles/sample}$; after folding, this equates to a spur moving from $0.5\,\text{cycles/sample}$ to $0.25\,\text{cycles/sample}$.

The second harmonics of each are shown in Fig. 17(c). Since both fundamental spurs are separated by $0.5\,\text{cycles/sample}$, their second harmonics appear superimposed after folding; since the second harmonics are half the height of the fundamental, the result is a spur that is the same height as the fundamental, moving a distance of $0.5\,\text{cycles/sample}$.[2]

[2]It should be noted that the prediction given up to this point does not indicate the initial position of the wandering spur harmonics, and these have been chosen after the fact so as to match the simulation result.

The third (Fig. 17(d)) and all q^{th} odd harmonics follow the same pattern as the fundamental, with the wander rate increased by a factor of q and the amplitude reduced by $20\log_{10}(q)$. Similarly, all q^{th} even harmonics follow the same pattern as the second harmonic. The wander rate in this case is increased by a factor of q, compared to the fundamental, but the amplitude is only reduced by $20\log_{10}(q/2)$ due to the superimposed spurs, as explained above for the second harmonic.

C. $b = 3$ *case*

Fig. 18 compares simulations and predictions for the same MASH modulator, with the input changed to $x = \lfloor M/3 \rfloor = 349525$. In this case, since $b = 3$, there appear to be three wandering spur groups, which are spaced in frequency by $f_{\text{PFD}}/3$.

Since $M/3$ is not an integer, the actual input is offset from the exact modulus fraction, thus producing wandering spurs. In this case, $x = (M/3) - (1/3)$. The wander rate of the spurs is therefore one third that seen in the previous case. The complete prediction, given by Eq. (35) in Appendix C, closely matches what is seen in simulation.

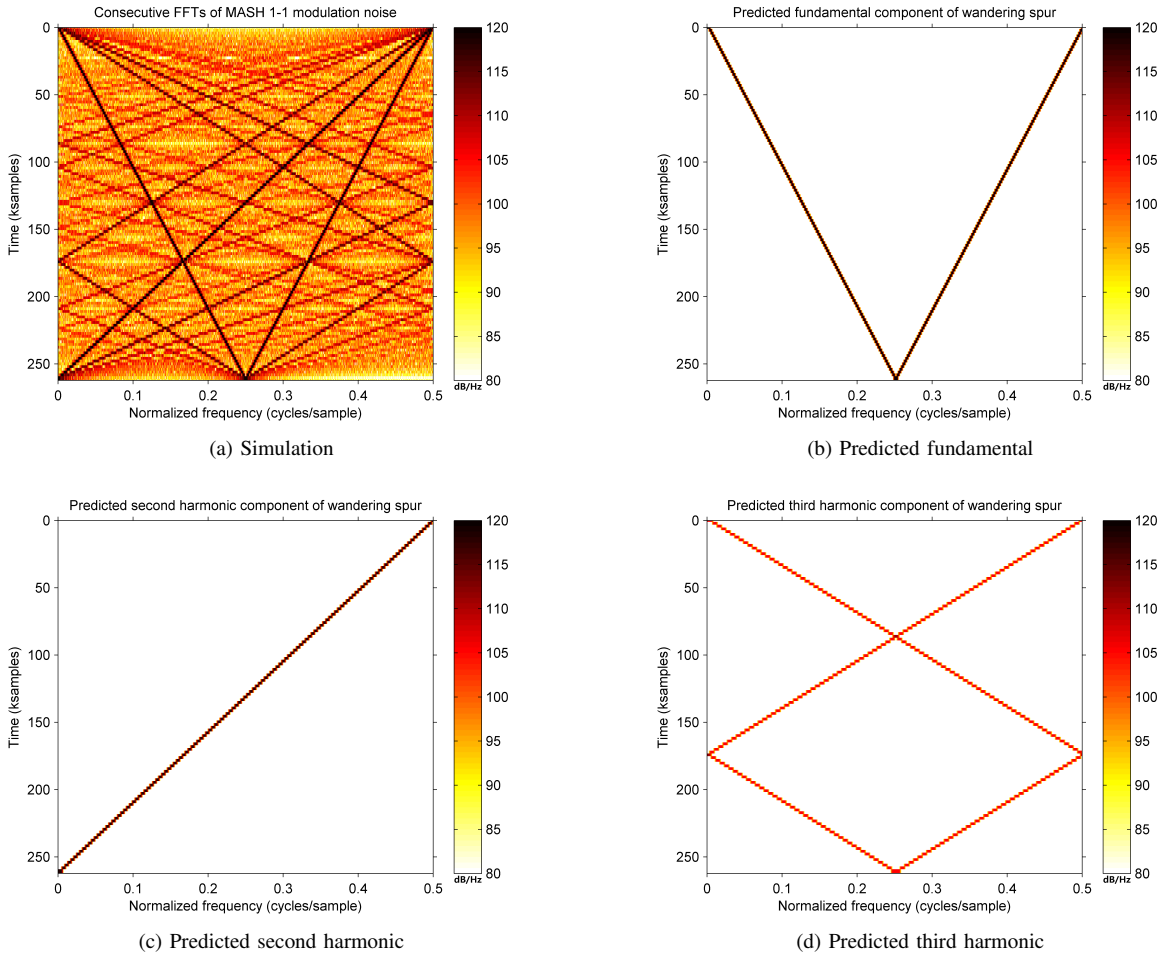

(a) Simulation

(b) Predicted fundamental

(c) Predicted second harmonic

(d) Predicted third harmonic

Fig. 17: Simulated MASH 1-1 spectrogram (a), and predicted fundamental (b) and second (c) and third (d) harmonic components of the wandering spur.

D. $b = 2$ with input dither case

Dithering is an effective technique for maximizing the cycle length of the DDSM modulator, and thus preventing spurs due to the deterministic operation of the modulator [9], [10]. Dithering can be applied to any DDSM in the MASH, and applying dither to later DDSM blocks has the beneficial effect of high-pass shaping the dither, thus moving the resulting noise power to the stopband of the loop response. Unfortunately, excessively shaped dither can itself cause spurs in the case of a fractional-*N* frequency synthesizer [9].

Pamarti and Galton have proven that only unshaped LSB dither can be applied to a MASH 1-1 if spur-free operation is required [9]. This corresponds to applying dither to the input of the MASH; if this dither is not zero-mean, the input mean is changed as a result, and this must be accounted for in the wandering spur prediction.

The modulator used previously was re-simulated with 1-bit uniform dither added to the input and the input set to $x = M/2$. The expected mean of the dither is 0.5; therefore, the average modulator input was offset by 0.5 from the modulus fraction.

Fig. 19 compares simulation, employing a binary pseudo-random noise source, and prediction, given by Eq. (37) in Appendix D. As expected, the wander rate in simulation has been reduced by a factor of two with respect to the situation in Section V-B where $x = 1$. Furthermore, the simulation and prediction match.

E. Large b case

It has previously been mentioned that wandering spurs are seen when the modulator input, x, is close to a fraction of the modulus, aM/b, where the denominator b is small. The prediction presented in (24) is by no means confined to this situation, and it can help explain why wandering spurs are not seen in practice for most values of x.

Fast-moving wandering spurs are not an interesting phenomenon, as they move too quickly to be visible during an observation window of any realistic length. Returning to the description of the wandering spur mechanism given in Section IV, we note that the input is defined as $x = aM/b + \bar{d}$, where a and b are co-prime integers and M is the modulus of the modulator. There will always be a way of choosing values of a and b that results in a small value of $|\bar{d}|$, which we have shown produces slow-moving wandering spurs. However, for

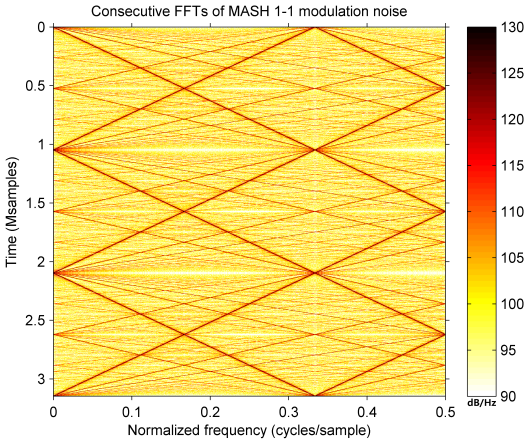

(a)

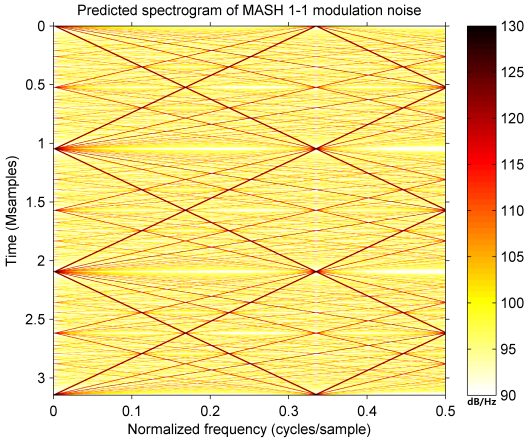

(b)

Fig. 18: Comparison between the output spectrograms from a MATLAB simulation of a MASH 1-1 (a) and from the prediction (b), where $x = \lfloor M/3 \rfloor$.

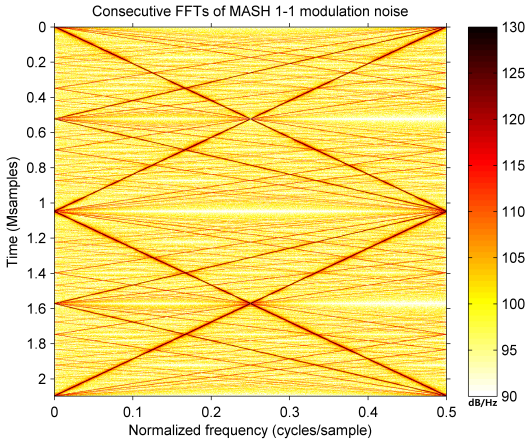

(a)

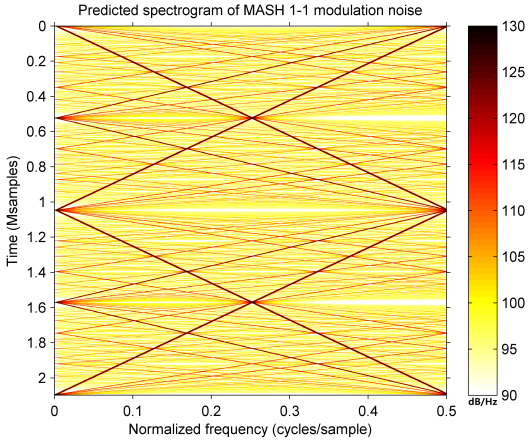

(b)

Fig. 19: Comparison between the output spectrograms from a MATLAB simulation of a MASH 1-1 with dither (a) and from the prediction (b), where $x = M/2$ and dither is applied.

most values of x, this will require choosing a large value of b, and hence a large number of spurs.

We have previously predicted that the fundamental components of the wandering spur groups are spaced equidistantly between 0 and $1\,\mathrm{cycles/sample}$. The spacing between each fundamental spur is therefore $1/b\,\mathrm{cycles/sample}$. If the value of b is large, the resulting spacing between spurs will be smaller than the frequency resolution of the measurement, and therefore distinct wandering spurs will not be visible.

An example is simulated in Fig. 20(a), where $x = M/128 + 1$. The prediction, given by Eq. (39) in Appendix E, anticipates 128 distinct moving spur groups. The predicted spectrogram is shown Fig. 20(b), where only the fundamental and 2nd and 3rd harmonics are shown. The wandering spur is not visible in these spectrograms. The reason for this is that a 2^{11}-point FFT is used, resulting in a frequency resolution of $0.49\,\mathrm{mcycles/sample}$, while there are 128 spurs, each spaced by $7.8\,\mathrm{mcycles/sample}$ in time. As can be seen in Fig. 21, the spurs are present, but too low in amplitude and two closely spaced to be clearly visible above the noise floor.

VI. Conclusion

In this paper we have demonstrated the occurrence of wandering spurs due to the use of a MASH 1-1 modulator. We have shown that the frequency modulation of the spurs is due to the architecture of the MASH, and we have derived analytical expressions for these spurs. Finally, we have demonstrated the validity of these expressions through simulation.

Appendix A
Prediction of spur amplitudes in Fig. 9

e_2 takes the form of a frequency-modulated sawtooth. Since frequency modulation does not influence the amplitude of the frequency components, we can refer to the decomposition of the sawtooth waveform [8]:

$$\frac{A}{\pi}\sum_{k=1}^{\infty}\left[\frac{(-1)^{k-1}}{k}\sin\left(2\pi k n\right)\right]. \tag{29}$$

In our case, $A = M/2 = 2^{17}$, and hence the amplitude of the k^{th} frequency component is given by

$$\frac{2^{17}}{k\pi}. \tag{30}$$

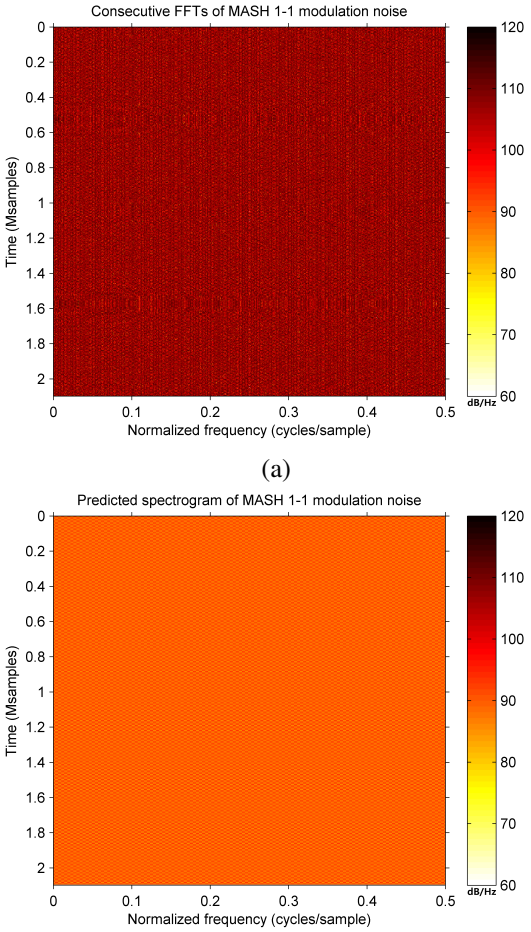

Fig. 20: Comparison between the output spectrograms from a MATLAB simulation of a MASH 1-1 (a) and from the prediction (b), where $x = M/128$.

which gives values of $92.4\,\mathrm{dB}$, $82.9\,\mathrm{dB}$ and $78.4\,\mathrm{dB}$ for the 1st, 3rd and 5th frequency components, respectively.

Each component has a wander rate of $k \times 7.8 \times 10^{-3}\mathrm{cycles/sample}$, while the 2^{11}-point FFT has a resolution of $0.488 \times 10^{-3}\mathrm{cycles/sample}$. The k^{th} frequency component is therefore spread over $16k$ bins. Consequently, the height of each ridge is reduced by $10\log_{10}(16k)\,\mathrm{dB}$. Additionally, the estimate should be scaled up by $20\log_{10}(N_{\text{FFT}})\,\mathrm{dB}$ to account for the FFT size, and finally scaled down by $10\log_{10}(N_{\text{FFT}})\,\mathrm{dB}$ to determine the power density.

This produces estimates of $113.5\,\mathrm{dB/Hz}$, $99.2\,\mathrm{dB/Hz}$ and $92.5\,\mathrm{dB/Hz}$ for the amplitudes of the 1st, 3rd and 5th frequency components, respectively, in the phase spectrum. Each of these will appear as ridges of widths $k \times 7.8 \times 10^{-3}\mathrm{cycles/sample}$ due to the differing wander rates, as explained in Section III.

Appendix B
Hamming window

The primary concern in choosing a suitable window is to conserve the amplitude of each spur. This was achieved through the use of a Hamming window, an 11-point version

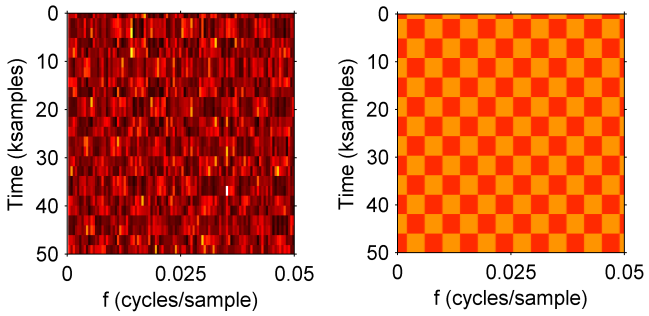

Fig. 21: Comparison between crops from the output spectrograms from Fig. 20, showing the presence of tightly-spaced spurs. The spurs are already difficult to distinguish in the simulated spectrum of e_2; with the contribution of other noise sources, the wandering spurs become indistinguishable from noise at the PLL output.

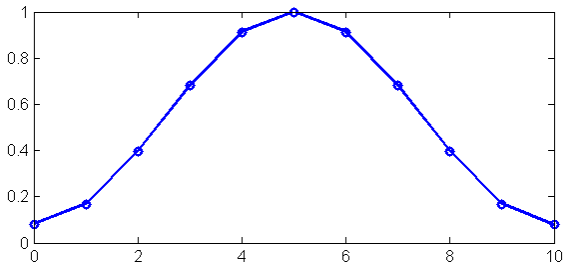

Fig. 22: 11-point Hamming window.

of which is shown in Fig. 22. This window is described by the function:

$$w[n] = 0.54 - 0.46\cos\left(\frac{2\pi n}{N-1}\right), \tag{31}$$

where N is the window length, and $0 \le n < N$.

If N is odd, then $N-1$ is even, and the maximum of the window lies at $n = (N-1)/2$, where:

$$w\left[\frac{N-1}{2}\right] = 1. \tag{32}$$

The window therefore preserves the amplitude of the spurs, while increasing the width of the spur peaks.

Appendix C
Prediction for $x = \lfloor M/3 \rfloor$

We begin by separating the input into a modulator fraction and an offset:

$$x = \left\lfloor \frac{M}{3} \right\rfloor \tag{33}$$

$$= \frac{M}{3} - \frac{1}{3}. \tag{34}$$

This gives us $b = 3$ and $\bar{d} = -1/3$. $M = 2^{20}$, as before. Substituting into Eq. (24), we obtain:

$$f_{e_2}^k[n] = \begin{cases} \dfrac{n}{2^{20}} - \dfrac{k}{3}, & 0 \leq \left(n - k \times 2^{20}\right) < n', \\ 1 - \dfrac{n}{2^{20}} + \dfrac{k}{3}, & n' \leq \left(n - k \times 2^{20}\right) < 2n', \end{cases} \tag{35}$$

where $n' = 3 \times 2^{19}$ and $0 \leq k < 3$.

APPENDIX D
PREDICTION FOR $b = 2$ WITH DITHERED INPUT

The input to the modulator without dithering is $M/2$. Additive dither with a mean of 0.5 is applied, and the resulting average input to the modulator is therefore:

$$x = \frac{M}{2} + \frac{1}{2}. \tag{36}$$

This gives us $b = 2$ and $\bar{d} = 0.5$. $M = 2^{20}$, as before.

Substituting into Eq. (24), we obtain:

$$f_{e_2}^k[n] = \begin{cases} \dfrac{n}{2M} - \dfrac{k}{2}, & 0 \leq (n - kM) < M, \\ 1 - \dfrac{n}{2M} + \dfrac{k}{2}, & M \leq (n - kM) < 2M, \end{cases} \tag{37}$$

where $0 \leq k < 2$.

APPENDIX E
PREDICTION FOR $b = 128$

The input is given by:

$$x = \frac{M}{128} + 1. \tag{38}$$

We therefore deduce that $b = 128$ and $\bar{d} = 1$. $M = 2^{20}$, as before.

Substituting into Eq. (24), we obtain:

$$f_{e_2}^k[n] = \begin{cases} \dfrac{n}{M} - \dfrac{k}{128}, & 0 \leq \left(n - \frac{kM}{128}\right) < \dfrac{M}{2}, \\ 1 - \dfrac{n}{M} + \dfrac{k}{128}, & \dfrac{M}{2} \leq \left(n - \frac{kM}{128}\right) < M, \end{cases} \tag{39}$$

where $0 \leq k < 128$. Note that the fundamental of each wandering spur group is separated by only $1/128 = 7.81\,\text{mcycles/sample}$ in frequency.

ACKNOWLEDGMENT

This work has been funded in part by the Irish Research Council, Science Foundation Ireland and Enterprise Ireland under grants GOIPG/2014/14222, 13/IA/1979 and 13/RC/2077, and T-2015-0019, respectively.

REFERENCES

[1] R. M. Gray, "Quantization noise spectra," *IEEE Transactions on Information Theory*, vol. 36, no. 6, pp. 1220–1244, Nov 1990.

[2] M. Perrott, M. Trott, and C. Sodini, "A modeling approach for Σ-Δ fractional-N frequency synthesizers allowing straightforward noise analysis," *Solid-State Circuits, IEEE Journal of*, vol. 37, no. 8, pp. 1028–1038, Aug 2002.

[3] B. De Muer and M. Steyaert, "A CMOS monolithic $\Delta\Sigma$-controlled fractional-N frequency synthesizer for DCS-1800," *Solid-State Circuits, IEEE Journal of*, vol. 37, no. 7, pp. 835–844, Jul 2002.

[4] M. Kennedy, H. Mo, Z. Li, G. Hu, P. Scognamiglio, and E. Napoli, "The noise and spur delusion in fractional-N frequency synthesizers," in *Proc. ISCAS 2015*, Lisbon, 24-27 May 2015.

[5] D. Mai, H. Mo, and M. P. Kennedy, "Observations and Analysis of Wandering Spurs in MASH-Based Fractional-N Frequency Synthesizers," *IEEE Transactions on Circuits and Systems II: Express Briefs*, vol. 65, no. 5, pp. 662–666, May 2018.

[6] E. P. Gonzalez and J. Reiss, "Idle tone behavior in sigma delta modulation," in *122nd Audio Engineering Society (AES) Conference*, 2007.

[7] B. Miller and B. Conley, "A multiple modulator fractional divider," in *44th Annual Symposium on Frequency Control*, May 1990, pp. 559–568.

[8] D. C. Champeney, *Fourier Transforms and Their Physical Applications (Techniques of physics)*. London: Academic Press, 1973.

[9] S. Pamarti and I. Galton, "LSB dithering in MASH delta-sigma D/A converters," *IEEE Trans. Circuits and Systems—Part I: Regular Papers*, vol. 54, no. 4, pp. 779–790, April 2007.

[10] V. R. Gonzalez-Diaz, M. A. Garcia-Andrade, G. E. Flores-Verdad, and F. Maloberti, "Efficient dithering in MASH sigma-delta modulators for fractional frequency synthesizers," *IEEE Transactions on Circuits and Systems I: Regular Papers*, vol. 57, no. 9, pp. 2394–2403, Sept 2010.

Yann Donnelly (S'14) received the B.E. degree in electrical and electronic engineering from University College Cork, Cork, Ireland, in 2014, and the Ph.D. degree from University College Cork in 2018. He is currently a Post-doctoral Research Fellow with University College Dublin, Dublin, Ireland, where his work focuses on techniques for mitigating spurious tones in fractional-*N* phase lock loops.

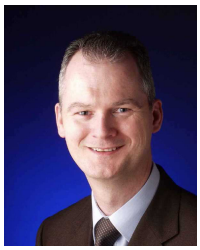

Michael Peter Kennedy (S'84-M'91-SM'95-F'98) received the B.E. degree in electronics from the National University of Ireland, Dublin, in 1984, and the M.S. and Ph.D. degrees from the University of California (UC Berkeley), Berkeley, in 1987 and 1991, and the DEng degree from the National University of Ireland in 2010. He was made an IEEE Fellow in 1998 for his contributions to the study of Neural Networks and Nonlinear Dynamics.

He worked as a Design Engineer with Philips Electronics, a Postdoctoral Research Engineer at the Electronics Research Laboratory, UC Berkeley, and as a Professeur Invité at the Federal Institute of Technology Lausanne (EPFL), Switzerland. From 1992 to 2000, he was on the faculty of the Department of Electronic and Electrical Engineering at University College Dublin (UCD), Dublin, Ireland, where he taught electronic circuits and computer-aided circuit analysis and directed the undergraduate Electronics Laboratory. In 2000, he joined University College Cork (UCC), Cork, Ireland, as Professor and Head of the Department of Microelectronic Engineering. He was Dean of the Faculty of Engineering at UCC from 2003 to 2005 and Vice-President for Research from 2005 through 2010. He returned to UCD as Professor of Microelectronic Engineering in 2017 where he is currently Head of the School of Electrical and Electronic Engineering.

He was a founding Director of Ireland's Microelectronics Industry Design Association in 2001 and has been Scientific Director of the Microelectronic Circuits Centre Ireland since 2010. He has over 390 publications in the area of nonlinear circuits and has taught courses on nonlinear dynamics and delta-sigma modulation in China, England, Greece, Hungary, Italy, Korea, Spain, Switzerland, and the USA. His research interests are in the simulation, analysis and design of nonlinear dynamical systems for applications in communications and signal processing.

Dr. Kennedy was the recipient of the 1991 Best Paper Award from the International Journal of Circuit Theory and Applications and the Best Paper Award at the European Conference on Circuit Theory and Design 1999. He served as Associate Editor of the IEEE TRANSACTIONS ON CIRCUITS AND SYSTEMS from 1993 to 1995 and from 1999 to 2004. He was awarded the IEEE Third Millennium Medal, the IEEE Circuits and Systems Society Golden Jubilee Medal in 2000, and the inaugural Parson's Medal for Engineering Sciences by the Royal Irish Academy (RIA) in 2001. He was elected to membership of the RIA in 2004, served as RIA Policy and International Relations Secretary from 2012 through 2016, and as President from 2017. He was Vice-President for Region 8 of the IEEE Circuits and Systems Society (CASS) from 2005 to 2007, a CASS Distinguished Lecturer from 2012 through 2013, and Chair of the CASS Distinguished Lecturer Program in 2017. He served on the IEEE Fellows Committee and the IEEE Gustav Robert Kirchhoff Award Committee.